

# Response of integral abutment bridges under a sequence of thermal loading and seismic shaking

Grigorios Tsinidis<sup>\*1,2</sup>, Maria Papantou<sup>3</sup> and Stergios Mitoulis<sup>4</sup>

<sup>1</sup>Department of Engineering, University of Sannio, Piazza Roma 21, Benevento, 82100, Italy

<sup>2</sup>Vienna Consulting Engineers ZT GmbH, Untere Viaduktgasse 2, 1030, Vienna, Austria

<sup>3</sup>AECOM, Structures & Bridges, One Trinity Gardens, Broad Chare, Newcastle upon Tyne, NE1 2HF, UK

<sup>4</sup>Department of Civil and Environmental Engineering, FEPS, University of Surrey, Guildford, GU2 7XH, UK

(Received August 3, 2018, Revised November 11, 2018, Accepted November 27, 2018)

**Abstract.** This article investigates the response of Integral Abutment Bridges (IAB) when subjected to a sequence of seasonal thermal loading of the deck followed by ground seismic shaking in the longitudinal direction. Particular emphasis is placed on the effect of pre-seismic thermal Soil-Structure Interaction (SSI) on the seismic performance of the IAB, as well as on the ability of various backfills configurations, to minimize the unfavorable SSI effects. A series of two-dimensional numerical analyses were performed for this purpose, on a complete backfill-integral bridge-foundation soil system, subjected to seasonal cyclic thermal loading of the deck, followed by ground seismic shaking, employing ABAQUS. Various backfill configurations were investigated, including conventional dense cohesionless backfills, mechanically stabilized backfills and backfills isolated by means of compressive inclusions. The responses of the investigated configurations, in terms of backfill deformations and earth pressures, and bridge resultants and displacements, were compared with each other, as well as with relevant predictions from analyses, where the pre-seismic thermal SSI effects were neglected. The effects of pre-seismic thermal SSI on the seismic response of the coupled IAB-soil system were more evident in cases of conventional backfills, while they were almost negligible in case of IAB with mechanically stabilized backfills and isolated abutments. Along these lines, reasonable assumptions should be made in the seismic analysis of IAB with conventional sand backfills, to account for pre-seismic thermal SSI effects. On the contrary, the analysis of the SSI effects, caused by thermal and seismic loading, can be disaggregated in cases of IAB with isolated backfills.

**Keywords:** bridge; long-span; integral abutment; thermal loads; seismic; soil-structure interaction

## 1. Introduction

Integral abutment bridges (IAB) are structures known for their low maintenance cost. An integral abutment is monolithically connected to the deck; thus no expansion joints or bearings are required at the end supports of the bridge, leading to significant cost savings in the long term (Mistry 2006, Mitoulis *et al.* 2010). This advantage explains the increasing application of IAB in short to medium-span bridges in railways and highways around the world (INTAB 2010, IABSE 2011). Integral abutments are either stub-type with steel piles (e.g., Quinn and Civjan 2016, LaFave *et al.* 2016) or reinforced concrete piles, or bank seat, or full-height frame or semi-integral abutments (Highways Agency 1995, 2000, 2001), all serving the same purpose, i.e., retaining the soil, supporting the bridge end span and providing a smooth transition to the bridge.

Despite the advantages of integral bridges, the rigid abutment-deck connection mandates that the abutments should be able to sustain the daily and seasonal thermal movements of the deck, as well as the movements resulting from other loadings, e.g., the seismic ground shaking. In

this context, these structural elements should be designed to be sufficiently flexible to sustain the aforementioned movements, yet having adequate vertical capacity to undertake the vertical loads of the bridge. Another critical design aspect is the long-term response of the backfills that are retained by the integral abutments. The movements of the abutments, associated to the aforementioned thermal and dynamic loading conditions, mobilize significant soil-structure interaction effects (SSI) that cause stress variations within the backfill soil and in turn result in densification, ratcheting (England *et al.* 2001) and settlements and/or swelling of the backfill soil (Helwany 2007), as well as build-up of the earth pressures acting on the abutments (Springman *et al.* 1996, England *et al.* 2000, Shamshabadi *et al.* 2007, Lemnitzer *et al.* 2009, Bloodworth *et al.* 2012). The above issues have been acknowledged in the international literature over the last 20 years (e.g., England *et al.* 2007, Hovarth 2010). Furthermore, the dynamic interaction effects between the IAB and the backfills during strong ground seismic shaking may lead to complex responses of the soil-bridge system (e.g., Zhang and Makris 2002, Kotsoglou and Pantazopoulou 2007, 2009, Shamsabadi *et al.* 2007, 2013, Aviram *et al.* 2008, Kappos and Sextos 2009, Tubaldi *et al.* 2010, Mitoulis 2012, Erhan and Dicleli 2015, Agalianos *et al.* 2017). These responses may be difficult to predict, when

\*Corresponding author, Ph.D.

E-mail: [tsinidis.grigorios@gmail.com](mailto:tsinidis.grigorios@gmail.com)

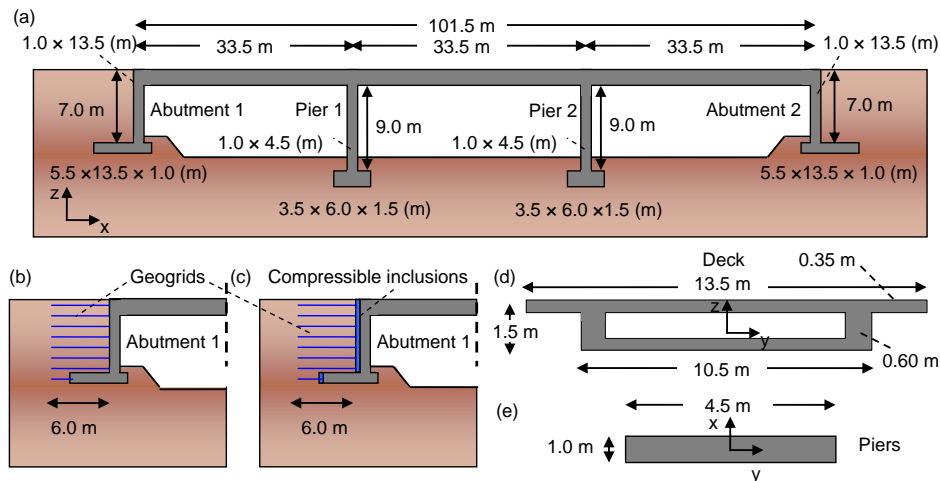


Fig. 1 IAB with (a) conventional backfills, (b) mechanical stabilized backfills, (c) compressible inclusions at the abutments and mechanically stabilized backfills. Cross sections of the (d) deck and (e) pier

significant thermal SSI effects have been preceded before the ground seismic shaking, particularly if someone accounts for deterioration effects caused by environmental factors (Zanini *et al.* 2013). As a result, design guidelines are found to be reluctant to promote rigid deck-abutment connections for bridges, especially in earthquake prone areas. For instance, Eurocode requires a behavior factor of one for locked-in structures (EN 1998-2 2005), e.g., IAB. The above design challenges become more intense with the increase of the length of the bridge. Hence, tackling these issues, to extend the length limits of IAB, has been a subject of research the recent years (Baptiste *et al.* 2011, Mitoulis *et al.* 2011).

Different designs have been proposed in the literature to address the aforementioned challenges in IAB. A displacement compensation unit has been patented by England (2005) to be implemented in integral bridges. Humphrey (2010), Humphrey and Blumenthal (2011) introduced the use of tyre derived aggregates as a compressible inclusion behind culverts to reduce the soil pressure on walls, whilst Athanasopoulos *et al.* (2012) have proposed the use of expanded polystyrene (EPS), which is being used extensively in modern bridge design concepts. Yet, EPS exhibits plastic deformations, hence allowing the wedging of the soil behind the abutment when the abutment moves toward the centre of the bridge. Argyroudis *et al.* (2016) conducted a numerical study to investigate the advantages of optimised sand and granulated rubber mixtures as backfills for IAB. It was found that this solution can potentially mitigate the seismic interaction effects between the IAB and the backfills. Mitoulis *et al.* (2016) has recently proposed an isolation scheme that includes novel compressible inclusions (CIs), made of reused shredded waste tyres, to be used for separation between the abutment and mechanically stabilized soil backfill.

Past research studies analyzed separately the effects of serviceability and seismic loadings on IAB, without examining their potential interaction. However, the serviceability loads mobilize SSI effects, which may change the stress state within the backfills, thus affecting the response of IAB during subsequent earthquake ground

shaking. Along these lines, this article aims at investigating the effect of inevitable pre-seismic thermal SSI on the seismic response of IAB. Emphasis is also placed on the capability of various backfills configurations, to minimize the dependence of seismic SSI effects on the thermal ones. The latter is of great interest to designers, as the potential decoupling of the SSI effects may allow the separate study of IAB under thermal and seismic loadings with a greater confidence and more importantly may extend the application of IAB into longer bridges. To shed light on the above issues, the response of a long IAB-backfills system subjected to a sequence of thermal loading of the deck, followed by seismic ground shaking, was numerically investigated by employing the finite element code ABAQUS. Various backfill typologies were studied, including conventional backfills, mechanically stabilized backfills, and backfills isolated by means of compressive inclusions. Critical characteristics of the investigated systems are discussed in the following sections on the basis of backfill responses and bridge resultants. Through the discussion, insights on the response of IAB-backfill systems under thermal movement of the deck are also provided.

## 2. Description of the case studies

### 2.1 Integral bridge-soil system

The IAB-soil system investigated herein is presented in Fig. 1(a). A three-span integral concrete bridge was considered. The total length of the bridge was 101.5 m, having a typical span of 33.5 m. The design of the bridge and the sizing of the structural elements, meet the Eurocode requirements (EN 1991-2 2003, EN 1997-1 2004, EN 1998-2 2004, EN 1998-5 2005). C30/37 concrete was considered for all the bridge structural elements, with a unit weight of  $25 \text{ kN/m}^3$ , Young's Modulus of 30 GPa and Poisson's ratio of 0.2. The deck was a prestressed box girder with a width of 13.5 m and a total depth of 1.5 m (Fig. 1(d)). The bridge had two integral piers, i.e., rigidly connected to the deck, and two full-height integral abutments. The integral

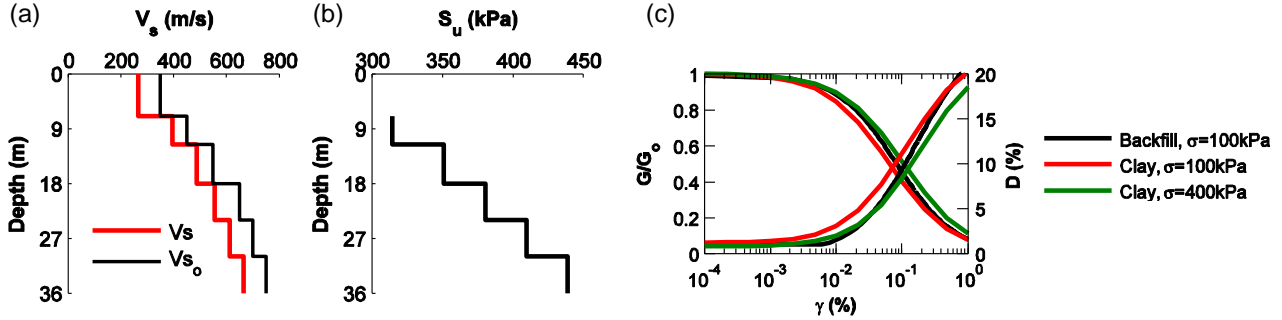


Fig. 2 (a) Small strain ( $V_{s0}$ ) and mean effective ( $V_s$ ) shear wave velocity gradients, (b) undrained shear strength ( $S_u$ ) gradient, (c)  $G$ - $\gamma$ - $D$  curves adopted in the one-dimensional soil response analyses

abutments had a width of 13.5 m and a thickness of 1.0 m and were founded on 5.5 m long spread footings with a thickness of 1.0 m, embedded 2.0 m below the ground surface. Wall-type piers, of transverse width equal to 4.5 m and height equal to 9.0 m, were considered for the bridge (Fig. 1(d)). The piers were founded on  $3.5 \times 1.0$  m footings, which were embedded 2.0 m below the ground surface. The dimension of the shallow foundations of the abutments was checked against realistic loads and displacements that were conservatively estimated for the case under consideration. Similar checks were conducted for the foundations of the bridge piers (i.e., check of bearing capacity and checks against sliding and overturning). The IAB-backfill system was founded on a very stiff clayey soil deposit of increasing stiffness and strength with depth, as per Section 2.2.

Three alternative backfill configurations were investigated, including conventional well-compacted backfills (Fig. 1(a)), mechanically stabilized backfills (Fig. 1(b)) and isolated backfills (Fig. 1(c)), to identify the importance of the sequence of thermal and seismic soil-structure interaction (SSI) effects on the response of IAB in various backfill configurations. In the latter two cases, the backfills were stabilized by means of geogrid layers, which were introduced horizontally at 0.5 m spacing. The length of these geogrid layers was 6.0 m from the abutments toward to backfill soil. In the case of the isolated backfills, compressible inclusions (CIs), made of reused shredded waste tyres with a thickness of 300 mm, were interjected between the vertical interfaces of the abutments and the backfill soil with the aim to separate the two components and disaggregate their responses. With reference to their technical application in practice; the inclusions are initially attached on the abutments with the construction of the layers of the backfill soil being followed. More details about this technique may be found in Mitoulis *et al.* (2016).

## 2.2 Backfill soil, foundation soil and CIs

Following a quite common practice in Europe and USA for IAB, the backfills were composed of a well-compacted cohesionless gravel-sand material. The selected material had a unit weight of  $18.5 \text{ kN/m}^3$  and Poisson's ratio of 0.43.

With reference to its strength properties; the backfill was characterised by friction angle  $\phi=42^\circ$ , and a dilatancy angle  $\psi=10.4^\circ$  (Schanz and Vermeer 1996). It is worth noticing that the selection of a cohesive backfill material would

probably lead to different effects of the thermal and seismic SSI on the performance of system, compared to a cohesionless backfill material, as the one examined herein.

The foundation soil was assumed to be a very stiff clay (soil class B, EN 1998-1 2004), having unit weight of  $19.5 \text{ kN/m}^3$  and Poisson's ratio of 0.35. The shear wave velocity, as well as the undrained shear strength ( $S_u$ ) of the soil deposit, were assumed to gradually increase with depth (Fig. 2). A series of one-dimensional soil response analyses were initially conducted to evaluate the mean soil equivalent properties, i.e. the degraded shear modulus and the damping, in the low to medium soil strains range. These properties were then introduced in the two-dimensional analyses of the entire system. The soil deposit was rested on elastic bedrock of unit weight  $20 \text{ kN/m}^3$  and shear wave velocity of 1,000 m/s.

The geogrids, employed in the case of the mechanically stabilized and isolated backfills, were assumed to have an axial stiffness of  $EA=10,000 \text{ kN/m}$ , where  $E$  and  $A$  are the elastic modulus and the cross-sectional area of the geogrids, respectively. A unit weight of  $6.1 \text{ kN/m}^3$  and Poisson ratio of 0.49 were considered for the compressible inclusions. The Young's modulus was set equal to 262.90 kPa, corresponding to an oedometric modulus of  $E_{oed}=4500 \text{ kPa}$  (Mitoulis *et al.* 2016).

## 3. Numerical modelling

The IAB models were analyzed by means of two-dimensional analyses, using the finite element code ABAQUS (2012). A unit transverse width of the coupled IAB-soil system was considered and analyzed under plane-strain conditions, as illustrated in Fig. 3. A sensitivity analysis was conducted, indicating that a soil grid of a total length of 280.0 m was adequate to reduce the potential boundary effects.

In particular, the soil, the footings of the piers and the abutments were meshed with quadratic plane-strain elements, while the piers and the deck were modelled by beam elements. The geogrids, implemented in cases of mechanically stabilized and isolated backfills, were simulated using truss elements, having stiffness  $EA=10,000 \text{ kN/m}$ . These elements can receive only tensile forces; thus they were activated only under tension. The size of the soil elements was selected, to ensure the efficient reproduction

of all the waveforms of the entire frequency range under study, i.e., frequencies during shaking in the range of 0.2 to 10 Hz, while meshing of the soil was generally finer in the vicinity of the abutments and the footings of the piers. Sections of generalized properties were used to simulate the mechanical properties of the deck and the piers, corresponding to the areas, second moment of areas and stiffnesses per unit width of the simulated bridges (due to the plane strain conditions adopted herein).

The rigid connection between the abutment and the deck, as well as between the piers and their footings was established by means of kinematic constraints (i.e., tie-type in ABAQUS), which were introduced between the nodes of the aforementioned structural elements. In particular, the nodes corresponding to the top 1.5 m of the abutments were rigidly connected with the deck node, to account for the depth of deck. With reference to the pier-deck connections, rigid links were introduced between the structural elements, to account for the eccentricity of the neutral axis of the deck from pier top.

The abutments-soil, footings-soil and compressive inclusion-soil interfaces were all modelled using a finite sliding hard contact algorithm, which is embedded in ABAQUS (2012). The model constrains the interacting media (i.e., soil and structural elements or soil and compressive inclusion elements) when are in contact, without transmitting tensile stresses to the interacting elements, while it also allows for potential separation. The tangential behaviour of the interfaces was modelled by introducing the Coulomb friction model. A friction coefficient,  $\mu=0.7$ , was assumed between the soil and foundation elements of the piers and abutments, as this is a typical value for clayey soil-concrete interfaces (e.g., Agalianos *et al.* 2017). Following Potyondy (1961), the friction coefficient for the backfill-abutment interfaces was set equal to  $\mu=\tan(0.76\times\varphi)$ , where  $\varphi$  is the friction angle of the backfill material. A slightly lower friction coefficient, i.e.,  $\mu=0.6$ , was assumed between the backfill-CI interfaces, based on the smoothness of the external surfaces of the CI.

The structural elements of the bridge, i.e., footings, piers, abutments and deck, were assumed to behave in an elastic manner. In this context, a linear elastic model was implemented for these elements, which was calibrated against the material properties mentioned in Section 2.1. The cracked flexural stiffness was adopted for the piers and the abutments, as per Eurocode 8 (EN 1998-2 2005). On the contrary, the uncracked stiffness of the deck was adopted in the analyses, given that this structural element is prestressed, thus is uncracked. The selection of the cracked flexural stiffness for the supporting elements of the IAB, affected, to some extent, the predicted response of the IAB under the thermal loading of the deck (where theoretically the gross flexural stiffness of the supporting elements should be considered); however, the selection was necessary to facilitate the sequential analysis of the system under thermal and seismic loadings. Moreover, the adopted elastic response of supporting elements is in line with the common design approaches for this type of structures (i.e., a behaviour factor  $q$  of up to 1.5 is commonly adopted).

A visco-elasto-plastic model was employed to simulate

the non-linear response of the soil, subjected to ground seismic shaking. The model, which combines a visco-elastic model with a non-associated Mohr-Coulomb material, both available in ABAQUS, was employed in the analyses, as follows; initially, a series of one-dimensional (1D) equivalent linear soil response analyses were conducted, to evaluate 'mean' effective soil equivalent properties for each soil layer (i.e. degraded shear modulus and viscous damping), corresponding to a medium soil strain range (e.g. the 'effective shear wave velocity' in Fig. 2(a)). The 1D soil response analyses were performed with code EERA (Bardet *et al.* 2000), by implementing adequate  $G-\gamma-D$  curves for the backfills and the foundation soil (Fig. 2(c)), Darendeli 2001, Pistolas *et al.* 2014). The equivalent soil properties were then introduced in the two-dimensional numerical model of the IAB-soil system. At that stage the yield strength of the soil was also defined, to account for the effect of soil nonlinearity for higher soil strain levels. The undrained shear strength  $S_u$  was used for the clayey foundation soil (Fig. 2(b)), while the strength properties discussed in Section 2.2 were used for the backfills. A slight cohesion, i.e.,  $c=1$  kPa, was introduced in the latter case to avoid numerical instabilities. The viscous damping (estimated by the 1D soil response analyses) was modelled in the form of the frequency-dependent Rayleigh type (Hashash and Park 2002). The Rayleigh coefficients were properly tuned for a frequency interval range, characterizing the 'dominant frequencies' of the soil deposit. The above soil modelling approach is commonly used by researchers (Evangelista *et al.* 2010, Callisto and Soccodato 2010, Tsinidis *et al.* 2015, 2016a, 2016b, Argyroudis *et al.* 2013, 2016) and practitioners due to its easy and efficient calibration and control.

The analyses were performed in steps, as follows; initially, the gravity field was established on the soil deposit, within a static step. The quasi-permanent action of the deck was also estimated, as per Eurocodes (EN1991-2 2003, EN1998-2 2005), adjusted per unit width and imposed on the deck as linear load. It is noteworthy that the static loads caused relatively small settlements to the foundations of the piers and the abutments, i.e., 5.0 to 6.0 mm, which are considerably smaller than the Eurocode requirements (i.e., 20 mm), thus, justifying the adequacy of the shallow foundations. After the introduction of the gravity and the quasi-permanent actions on the IAB, a cyclic expansion-contraction thermal loading was imposed on the deck in consecutive steps, resulting in cyclic movements of the abutments towards or away from the backfills. Generally, the daily and seasonal temperature changes are random, thus causing random thermal deformations on the deck and subsequently on the abutments (England 2000). In this study, only the seasonal thermal changes were considered, since the daily ones are smaller and hence mobilise less significant interaction effects than seasonal changes. The consideration of the daily thermal deformations on the deck and the abutments might have added some additional SSI effects that could potentially bias to some minor extent the presented results. However, taking into account the random nature of these daily changes, their definition and introduction in the

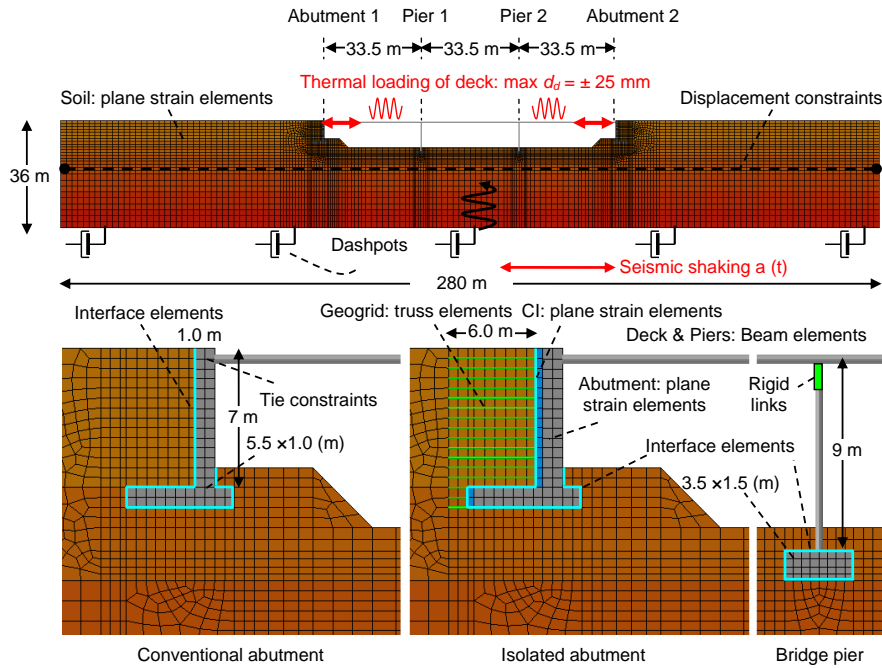


Fig. 3 Layout and details of the numerical models of the IAB-soil configurations

analysis would have complicated significantly the study. In particular, 20 full cycles of thermal expansion and contraction of the deck were considered, as a reasonable pre-seismic serviceability loading of the bridge. These 20 cycles correspond to the thermal loading condition of 20 years for the deck, referring to a uniform temperature range of  $\pm 25^\circ\text{C}$ , as per Eurocode 1 (EN1991-5 2003). Based on the length of the bridge and the adopted coefficient of thermal expansion for the concrete, i.e.,  $\alpha=10^{-5}/^\circ\text{C}$ , the above temperature range resulted in a maximum displacement of  $\pm 25$  mm at the monolithic abutment-deck connection. The thermal loading started with expansion of the deck. A sensitivity analysis indicated that for a number of thermal cycles larger than 15-20, the sequence of expansion or contraction of the deck did not affect drastically the predicted soil-structure interaction effects and therefore the computed response of the IAB and the backfills. The variation of the thermal displacement did not account for the temperature gradients applied on the deck nor the effects of prestressing, creep and shrinkage, phenomena that generally cause a reduced permanent shortening of the deck and a slight dislocation of the abutments. The above simplifications were made to investigate the net influence of thermal loading of the deck on the seismic behaviour of the IAB-backfills system.

The seismic loading was introduced after the completion of the cyclic thermal loading of deck, within a final implicit dynamic step. In particular, the ground motions were introduced at the base boundary of the numerical model, in terms of acceleration time histories, as per Fig. 3. Additional dynamic analyses were performed, neglecting the thermal loading before ground seismic shaking. The predictions of the latter analyses were compared with the cases, where the thermal loading was considered.

During the ‘gravity-geostatic’ and ‘thermal loading’ steps, the base of the numerical model was fixed in both

horizontal and vertical directions. In the subsequent ‘earthquake’ dynamic step, the horizontal direction of the base was released and the seismic shaking motions were applied on the model, as vertically propagated shear waves, through appropriate horizontal dashpots, the latter defined as per Lysmer and Kuhlemeyer (1969) on the basis of the mass density,  $\rho$ , and shear wave velocity,  $V_s$ , of the underlying bedrock (i.e.,  $V_s=1,000$  m/s and  $\rho=2.2$  t/m<sup>3</sup>). Kinematic tie constraints were set at the side boundaries of the model (displacements constraints shown in Fig. 3), allowing for common lateral displacement patterns, throughout the analysis procedure. This boundary condition imitates the desirable ‘shear beam’ response of free-field soil during ground seismic shaking.

It is worth noticing that the 2D simulation of the investigated systems constitutes an approximation of the actual problem. However, the use of a rigorous 3D model would require significant computational effort, precluding the potential to perform a detailed parametric study to gain a deeper understanding of the problem. Since the corresponding areas, second moment of areas and stiffnesses of the structural elements of the IAB are all adjusted per unit width, the selection of 2D simulation of the IAB is not expected to affect the computed structural response. Additionally, the efficiency of an equivalent 2D model to replicate the 3D response of the abutment-backfill system has been verified recently by Agalianos *et al.* (2017).

#### 4. Seismic input motions

Seven real acceleration time histories (Table 1), scaled to  $\text{PGA}=0.30$  g, were used as input shaking motions for the analyses. The selected input shaking motions were recorded to conditions similar to ‘seismic’ bedrock (i.e., ground type

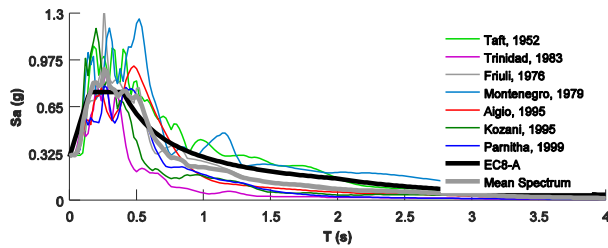


Fig. 4 Elastic response acceleration spectra of the seismic input motions (for 5% of critical damping) as compared to the Eurocode 8 (EN 1998-1 2004) response acceleration spectrum, corresponding to soil class A, all scaled to 0.3 g

A (rock) or B (stiff soil), according to Eurocode 8 (EN 1998-1 2004) and varied in amplitude, frequency content and significant duration of the seismic excitation. The ground motions were selected, so as their mean spectrum to match the Eurocode 8 spectrum for ground type A in the range of periods 0.15 s to 0.40 s, as shown in Fig. 4. Preliminary modal analyses, carried out assuming an elastic soil response, yielded a fundamental period of 0.29 s for the conventional bridge-backfills system, when the mass of the backfills was taken into account in the analyses. The fundamental period of the system was decreased to approximately 0.23 s when the mass of the backfills was neglected.

## 5. Results

### 5.1 Response of backfills

The response and permanent deflection of the backfills were assessed for both the cyclic thermal loading of the deck and the subsequent ground seismic shaking. Fig. 5 illustrates typical deformed shapes of the left-side backfill-abutment systems (i.e. abutments 1 in Fig. 3), predicted by the numerical analyses at distinct time steps of maximum thermal expansion or contraction of the deck. To highlight the differences on the predicted responses, the deformed shapes are amplified by a scale factor of 10. Generally, the seasonal cyclic thermal movement of the deck results in a built-up of residual vertical deflections of the backfills (i.e.,

Table 1 Seismic shaking motions used in this study

Earthquake	Station ID-Station name	Magnitude, $M_w$	PGA (g)
Pamitha, Greece, 7/9/1999	2472-Athens 4 (Kipseli District)	6.0	0.12
Kozani, Greece, 13/5/1995	ST1320 - Prefecture building	6.5	0.14
Aigio, Greece, 15/6/1995	Telecommunication building	6.5	0.54
Friuli, Italy, 6/5/1976	ST20-Tolmezzo-Diga Ambiesta	6.4	0.32
Montenegro, 15/4/1979	ST64	6.9	0.18
Taft, USA, 21/7/1952	Santa Barbara, Courthouse	7.3	0.20
Trinidad, USA, 24/8/1983	090 CDMG station 1498	5.5	0.19

heaving and settlements). This observation is by far more evident in the case of the conventional backfill (Fig. 5(a)). In particular, when the abutment moves away from the backfill (i.e., thermal contraction of the deck), the backfill yields and moves downwards (settles), especially near the backfill-abutment interface. During the expansion of the deck, the abutment moves towards the backfill, which, due to its high dilation (well compacted cohesionless material) and previous yielding response, swells, leading to a residual upward deflection. The cyclic thermal movements of the deck result in residual upward deformations on the surface of the mechanically stabilized backfill, as well (Fig. 5(b)); however, these deformations are reduced compared to the conventional backfill, due to the contribution of the geogrids. Indeed, when the abutment moves away from the backfill, i.e., during deck contraction, the geogrids ‘support’ the backfill, reducing its yielding and associated permanent deformations. On the contrary, for a movement of the abutment towards the backfill, i.e., during deck expansion, the geogrids follow the backfill deformation, without contributing on the response. The deformation level during this state is generally reduced, compared to conventional backfill, due to the lower yielding response of the stabilized backfill. The yielding response of the backfill is further discussed in the ensuing. The introduction of the compressive inclusions between the abutment and backfill

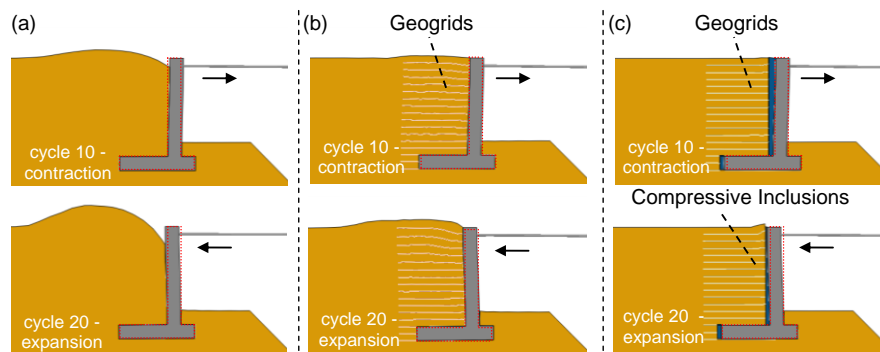


Fig. 5 Deformed shapes of left-side abutment-backfill configurations of IAB with (a) conventional backfills, (b) mechanically stabilized backfills, (c) mechanically stabilized backfills supported by isolated abutments. Note: dashed lines show initial positions of the abutment (scale factor  $\times 10$ )

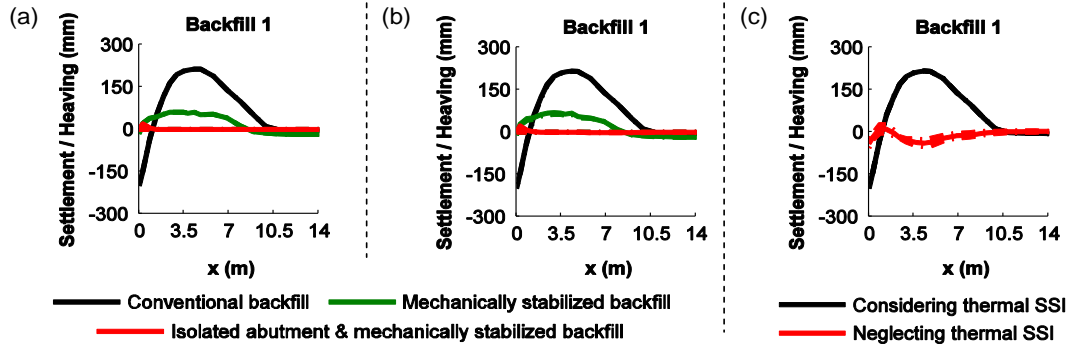


Fig. 6 Residual vertical deflections of the surfaces of the left-side backfills computed (a) at the completion of 20 full cycles of expansion and contraction of the deck, and (b) the completion of the seismic ground shaking followed the cyclic thermal loading; (c) comparisons of mean  $\pm 1$  standard deviation distributions of surface residual vertical deflections, computed on the conventional backfills when considering or neglecting the pre-seismic thermal SSI effects

(Fig. 5(c)) results in a significant reduction of the permanent deflections of the backfill. Actually, a reduced swelling deflection is observed at the top of the backfill-compressive inclusion interface, which is associated to local yielding of the soil at this location. The response of geogrids in the isolated backfill is similar to the one described for the mechanically supported backfill; however, their contribution is lower here, due to the reduced interaction between the abutment and the backfill.

Fig. 6(a) compares the residual surface vertical deflections of the left-side backfill configurations, computed at the completion of the cyclic thermal expansion and contraction of the deck. The comparisons refer to a distance up to 14.0 m from the abutments ( $x$  in the graphs stand for the distance from the abutments). The results for the conventional backfill indicate residual settlements between  $x \approx 0.0$ -1.5 m from the abutment, which reach a maximum of -180 mm at the abutment-backfill interface. For  $x \approx 1.5$ -10.5 m, the backfill exhibits swelling deflections, reaching a maximum displacement upward of 220 mm. After a transition zone of 11.0 m from the abutment, the backfill exhibits negligible vertical deflections. The mechanically stabilized backfill exhibits swelling deformations for a distance up to  $x \approx 7.0$ -8.0 m from the abutment, reaching a maximum of 70 mm. The mechanically stabilized backfill, supported by the isolated abutment, exhibits much lower swelling distortions (maximum 30 mm at the backfill-abutment interfaces), which are distributed up to a distance  $x \approx 0.5$  m. Similar responses were observed for the right backfills.

Fig. 6(b) compares the mean distributions of post-seismic residual vertical deflections of the left-side backfill surface, computed by the deflections calculated for the individual earthquake excitations. The computed deflections that account for the pre-seismic thermal SSI effects are similar to those referring only to the pre-seismic thermal SSI. Hence, it is evident that the pre-seismic thermal SSI effects dominate the residual deformations of the backfills, while the seismic SSI effects have a reduced contribution on the total residual deformations after earthquake.

Fig. 6(c) compares the post-shaking residual deflections of the conventional left-side backfill surface, computed when considering or neglecting the pre-seismic SSI effects.

The comparisons focus on the conventional backfill, since the effects of both the thermal and seismic SSI effects are more pronounced in this case. The solid lines correspond to the mean distributions of the deflections ( $\mu$ ), computed by the deflections of the individual earthquake excitations. The dashed lines, presented when the pre-seismic thermal SSI effects are neglecting, stand for the mean value plus/minus one standard deviation ( $\mu \pm 1\sigma$ ) distributions of the deflections computed by distortions calculated by the individual earthquake excitations. The relevant  $\mu \pm 1\sigma$  distributions coincided with the mean distributions in the case where the pre-seismic SSI effects were considered, indicating a minor effect of shaking loading characteristics on the distortions for these cases. The above observations indicate a prevailing effect of the pre-seismic thermal SSI on the post-seismic residual deflections of the backfills.

In particular, when thermal SSI effects are considered, a post-seismic residual settlement is reported between  $x \approx 0.0$ -1.5 m from the abutment, reaching a maximum of 190.1 mm at the abutment-backfill interface. For  $x \approx 1.5$ -10.5 m, the backfill exhibits a swelling deflection, reaching a maximum of 229.8 mm. When the pre-seismic thermal SSI effects are neglected, the predicted post-shaking residual deformation is significantly lower (i.e., around one fifth of the distortions predicted when considering the thermal SSI) and distributed in a quite distinct fashion. More specifically, a maximum residual settlement of  $40.0 \text{ mm} \pm 15.5 \text{ mm}$  is reported at the soil-abutment interface, with  $\pm 15.5 \text{ mm}$  being the standard deviation of the permanent deflection. After this abrupt settlement, a residual swelling of the backfill is observed, reaching its maximum value, i.e.,  $10.8 \text{ mm} \pm 8.5 \text{ mm}$ , at a distance 0.8 m behind the abutment. A residual settlement of  $39.1 \text{ mm} \pm 12.6 \text{ mm}$  is reported at a distance of 4.3 m behind the abutment. Similar observations were made for the right-side backfill.

As stated, the above residual distortions of the backfills are attributed to the densification and yielding phenomena caused by the thermal and seismic SSI effects. Fig. 7 highlights the yielding response of the backfills caused by the thermal SSI effect, by plotting representative distributions of the accumulated soil plastic strains (i.e., resultant of the plastic strain tensor), computed in the investigated backfill configurations after the completion of

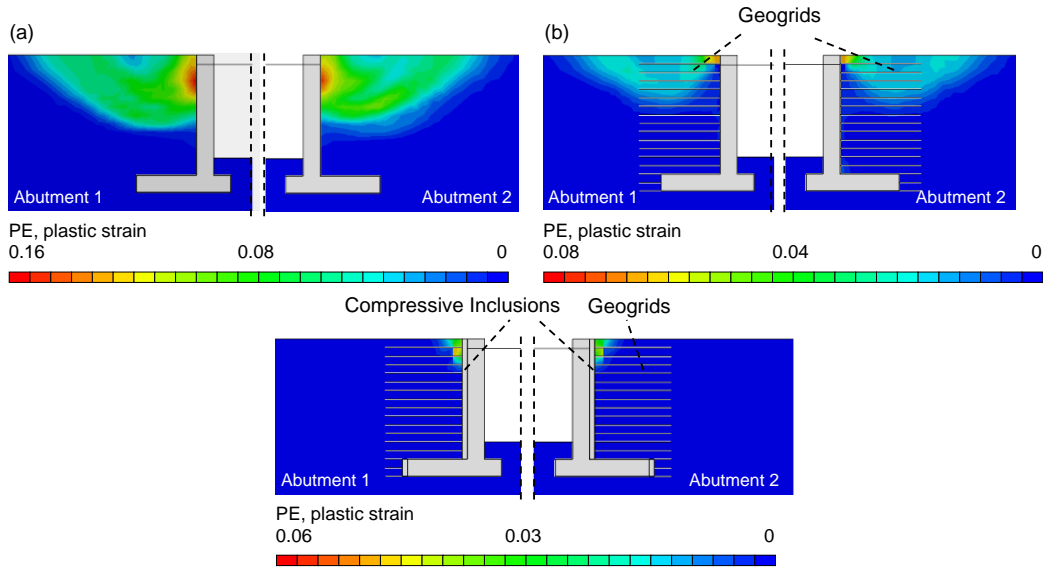


Fig. 7 Soil plastic strain distributions computed at the completion of cyclic thermal loading of the deck in (a) the conventional backfills, (b) the mechanically stabilized backfills, (c) the mechanically stabilized backfills with isolated abutments

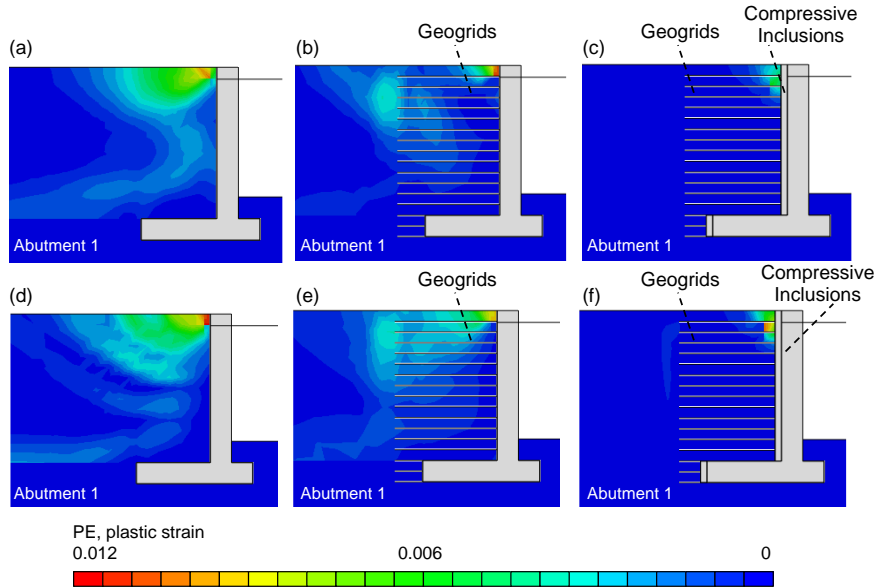


Fig. 8 Distributions of dynamic soil plastic strains computed at the completion of shaking with the record from the Athens earthquake, when neglecting (a-c) or considering (d-f) the pre-seismic thermal SSI effects

20 cycles of thermal expansion and contraction of the deck. The results indicate significant plastic strains at the top of the conventional backfills and up to a distance of 10.0 to 12.0 m from the abutments. The contribution of the geogrids, in case of mechanically stabilized backfills, results in lower plastic strains within the backfills, which are distributed in a narrower area (compared to the conventional backfills), near the ground surface. The plastic strains predicted in case of mechanically stabilized backfills, supported by isolated abutments, are considerably reduced and are mainly concentrated at the backfill soil-compressive inclusions interfaces near the ground surface. It is worth noticing that the plastic strain distributions computed on left-side and right-side backfills are rather symmetric; however, some differences are observed in case of conventional backfills.

Similar to the thermal effects, the ground seismic shaking mobilizes significant SSI effects that result in yielding of the backfills. Fig. 8 plots representative distributions of the plastic strains of the backfills computed at the completion of ground seismic shaking with the Parnitha record from the Athens earthquake (Table 1), when considering or neglecting the thermal SSI effects. The presented results correspond to the effect of seismic loading only (i.e., dynamic soil plastic strains), neglecting any effect of the pre-seismic soil plastic strains caused by thermal SSI effects when the latter are considered. Generally, the soil plastic straining caused by seismic ground shaking is much lower than the one predicted for the cyclic thermal movement of the deck. This observation explains the dominance of thermal SSI effects on the residual deflections of the backfills, discussed above.

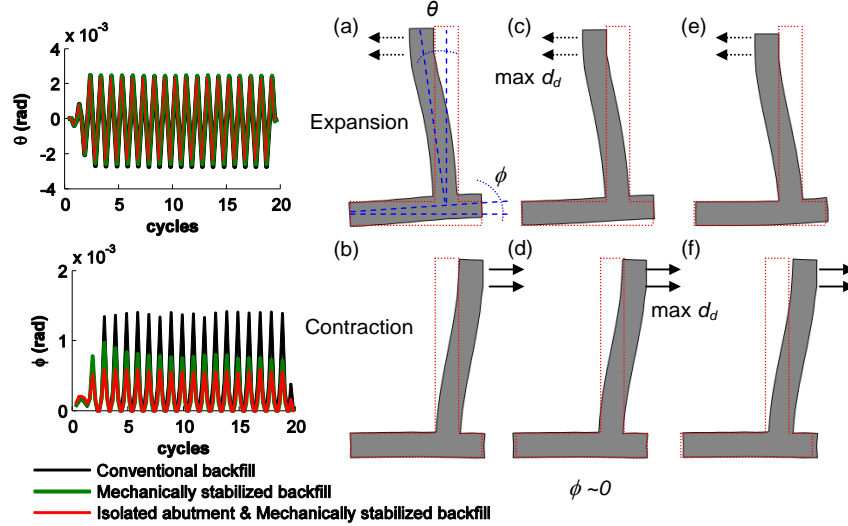


Fig. 9 Deformed shapes of the left abutments with (a, b) conventional backfills, (c, d) mechanically stabilized backfills, (e, f) isolated, mechanically stabilized backfills, caused by thermal expansion and contraction of the deck

Comparing the responses for the various investigated backfill configurations, conventional backfills exhibit significant dynamic soil plastic strains, which are distributed in a wide area of the backfills (Fig. 8(a)). The dynamic soil plastic strains are reduced in case of mechanically stabilized backfills and are distributed in a narrower area near the ground surface (Fig. 8(b)). The dynamic soil plastic strains predicted in case of a mechanically stabilized backfill and isolated abutment are significantly lower and are concentrated near the interface at the top surface (Fig. 8(c)). The consideration of pre-seismic thermal loading of the deck results in an increase of the dynamic soil plastic strains, compared to the cases where thermal SSI effects are neglected. The latter observation is particularly evident in cases of conventional (Fig. 8(d)) and mechanically stabilized backfills (Fig. 8(e)).

### 5.2 Deformation patterns of abutments during thermal loading of the deck

The cyclic thermal movement of the deck induces significant deformations on the integral abutments. Fig. 9 illustrates typical deformed schemes of the left abutment, i.e., abutment 1 in Fig. 3, computed at maximum thermal expansion or contraction of the deck. The deformed shapes, which refer to all examined backfill configurations, are plotted with a scale factor  $\times 50$ , to highlight clearly the differences on the deformation patterns. Time histories of the drifts of the abutments walls (i.e.,  $\theta$  time histories) are comparatively displayed in the same figure. These are computed, as

$$\theta(t) = (d_{top}(t) - d_{base}(t)) / h \quad (1)$$

where  $d_{top}(t)$ ,  $d_{base}(t)$  are the time histories of horizontal deformation of the top and base of the wall of the abutment, respectively, and  $h$  is the height of the wall of the abutment. Time histories of the rocking response of the abutments footings (i.e.,  $\phi$  time histories), are also presented in the same figure.

Under the thermal expansion of the deck, all examined abutments are forced to tilt toward the backfills. The abutments with the mechanically stabilized backfills, as well as the isolated abutments, exhibit slightly lower drifts compared to the abutments with conventional backfills. The effect of backfill configuration is more evident on the rotational response of the abutments footings. During the thermal expansion of the deck, the footing of the abutment with the conventional backfill (Fig. 9(a)) exhibits much higher rotation compared to the mechanically stabilized backfill (Fig. 9(b)). The footing of the isolated abutment exhibits the lowest rocking response, i.e., 65% lower rotation compared to the abutment with the conventional backfill (Fig. 9(c)). During the thermal contraction of the deck, the abutments move away from the backfills, with the footings practically exhibiting no uplifting, due to the significant weight of the supported backfills. As discussed in Section 5.4, these deformation patterns result in significant earth pressures on the walls of the abutments during the cyclic thermal loading of the deck.

### 5.3 Seismic drifts of abutment walls

The abutments of the IAB exhibit significant drifts during ground seismic shaking that induce high bending moments on their walls (see Section 5.5). Table 2 summarizes representative values of the maximum drifts of the left-side abutments computed for the various backfill configurations during ground seismic shaking, considering or neglecting the pre-seismic thermal SSI effects.

For most of examined cases, the consideration of the pre-seismic thermal SSI effects results in a slight decrease of the maximum seismic drifts of the walls of the abutments with conventional backfills, with this decrease reaching a maximum of 10%. This observation should be attributed to the yielding response of the backfills, which is mobilized during the pre-seismic thermal SSI effects and changes the stress states within the backfills, thus affecting the support that is offered on the abutments during the subsequent

Table 2 Maximum drifts of the left-side abutments computed during representative ground shaking motions, when considering or neglecting the pre-seismic thermal SSI effects

Backfill configuration	Pre-seismic thermal SSI effects	Ground seismic motion		
		Friuli 1976	Montenegro 1979	Parnitha 1999
Drift of abutment with conventional backfill (%)	yes	0.18	0.18	0.12
	no	0.18	0.19	0.13
Drift of abutment with stabilized backfill (%)	yes	0.15	0.16	0.12
	no	0.16	0.16	0.13
Drift of abutment with isolated backfill (%)	yes	0.33	0.31	0.25
	no	0.33	0.31	0.25

ground seismic shaking.

The drifts of the abutment with the mechanically stabilized backfill are generally lower than those predicted for abutment with the conventional backfill (i.e., differences up to 9 %). Similar to the abutment with the conventional backfills, the thermal SSI effects result in a reduction of the abutment drift compared to the case where this thermal loading is not considered.

Much higher drifts are reported in the case of the isolated abutment compared to those predicted for the IAB with conventional abutments. This is due to the decoupling between the backfill soils and the bridge that is offered by the compressive inclusions. The IAB can deform more easily during ground seismic shaking, hence inducing higher displacements and drifts on the abutments. Additionally, the effect of pre-seismic thermal SSI effect on the seismic drifts of the isolated abutments is negligible. Similar observations were made for the abutments on the right-side, i.e., abutments 2 in Fig. 3, as well as for the piers.

#### 5.4 Earth pressures on the abutments

Fig. 10 portrays representative earth pressure time histories computed on the examined abutments at a depth of 1.5 m below the ground surface. In particular, Fig. 10(a) shows the earth pressure time histories computed during the cyclic thermal expansion and contraction of the deck. Fig. 10(b) presents typical seismic earth pressure time histories (i.e., dynamic part of the earth pressures) computed when considering the pre-seismic thermal SSI effects. Fig. 10(c) highlights the importance of pre-seismic thermal SSI effects on the seismic earth pressures developed on the abutments, by comparing representative seismic earth pressures time histories computed by either considering or neglecting the pre-seismic thermal SSI effects. The earth pressures time histories that are plotted in Figs. 10(b)-(c) refer to ground seismic shaking of the 1999 Parnitha earthquake record, scaled to  $PGA=0.30$  g.

The cyclic thermal movement of the deck cause a fluctuation of earth pressures on the abutments walls (Fig. 10(a)). In particular, the thermal expansion of the deck causes a high reaction of the conventional backfills, which

is expressed by the development of significant earth pressures on the abutments (as high as 1,000 kPa/m in the case examined herein). It is worth noticing the differences on the maximum earth pressures predicted on the two abutments. This is attributed to the differences on the yielding response of the opposite backfills during the cyclic thermal loading of the deck (Fig. 7). Significant residual earth pressures are also identified at the completion of the cyclic thermal loading, reaching 500 kPa/m. These residual pressures should be attributed to the significant yielding of the conventional backfills (see Section 5.1). Similar observations are made for the mechanically stabilized backfills, with the maximum and residual earth pressures being reduced, however, to 600 kPa/m and 25 kPa/m, respectively. The maximum and residual earth pressures are further decreased to less than 200 kPa/m and 20 kPa/m, respectively, in case of mechanically stabilized backfills with the isolated abutments.

With reference to the seismic earth pressures; the time histories computed on the opposite abutments of the same IAB are out of phase, i.e. when one of the abutments moves toward the backfill the other abutment is pulled away from the backfill (Fig. 10(b)). Generally, the magnitude of the seismic earth pressures is fluctuating significantly during ground shaking, while residual earth pressures are observed after the excitation. The maximum seismic earth pressures at the examined depth can be as high as 250 kPa/m and 480 kPa/m for the conventional and the mechanically stabilized backfills, respectively. The aforementioned values are much higher than the maximum earth pressures developed on the isolated abutments, which do not exceed 110 kPa/m. Similar observations are made by comparing the residual earth pressures computed for the examined backfill configurations. The abutments with the conventional backfills receive a post-seismic residual pressure of 150 kPa/m, while the isolated abutments experience the lowest post-shaking residual earth pressures, i.e., 15 kPa/m.

The evolution of the seismic earth pressures is affected by the pre-seismic thermal SSI effects, particularly in the cases of conventional and mechanically stabilized backfills (Fig. 10(c)). This is generally expected, since the pre-seismic thermal SSI effects mobilize significant yielding on the backfill configurations, which result in changes on the stress states within the backfills and in turn changes on the support that is being offered on the abutments during the subsequent seismic shaking. The introduction of the compressive inclusions and the associated decoupling of the backfills from the abutments, result in a more elastic response of the backfills, making the effect of thermal SSI on the seismic SSI almost negligible.

Fig. 11(a) compares the residual earth pressures distributions computed on the abutments at the completion of the cyclic thermal loading of the deck. Similar distributions are predicted on opposite abutments for all the examined backfill configurations. In particular, higher residual earth pressures are reported on the upper part of the abutments with the conventional backfills, i.e., from the mid-height of the abutment to its top. The earth pressures reach a maximum of 690 kPa/m at a depth of 1.50 m from the ground surface. On the contrary, higher residual earth pressures are observed at the lower part of the abutment,

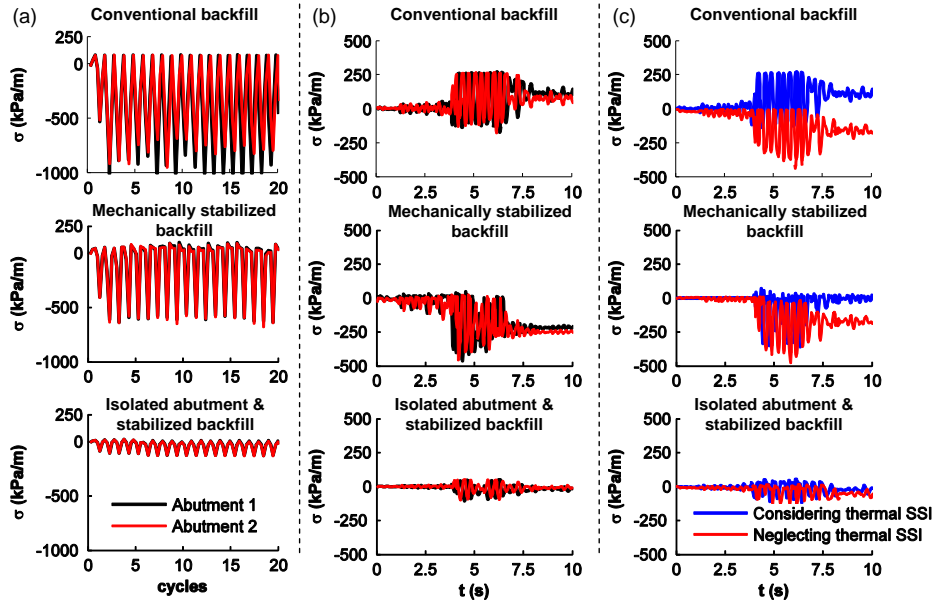


Fig. 10 Time histories of earth pressures computed at a depth 1.5 m below the ground surface. (a) Earth pressures due to cyclic thermal loading of the deck. (b) Seismic earth pressures for the Parnitha record, scaled to 0.30 g, considering the pre-seismic thermal SSI effects. (c) Effect of pre-seismic thermal SSI on the seismic earth pressures computed for shaking motion with the Parnitha record, scaled to 0.30 g

i.e., from the footing to the mid-height of the abutments, in case of mechanically stabilized backfills. However, the maximum earth pressures in this case do not exceed 350 kPa/m. The isolated abutments experience the lowest residual earth pressures, with a maximum value of 125 kPa/m, being reported at the base of the wall of the abutment.

Fig. 11(b) portrays comparisons of post-seismic residual earth pressures distributions. The presented results account for the thermal SSI effects prior to the earthquake excitation and correspond to mean distributions (solid lines in Fig. 11(b)) and mean value plus/minus one standard deviation distributions (dashed lines in Fig. 11(b)) of the residual earth pressures calculated for the individual earthquake excitations. Generally, the post-seismic residual earth pressures are lower than those predicted after the cyclic thermal movement of the deck. Additionally, some differences are observed between the distributions computed on the opposite abutments, due to the inherent asymmetry of the shaking motions, i.e., larger displacement amplitudes are induced towards one direction of the system. More specifically, the residual earth pressures computed behind abutments with conventional backfills are increased near the abutment-deck connections. This increase is associated to the high pre-seismic residual earth pressures at this location, caused by the thermal SSI effects, in addition to the large deformations and movement of the abutments, caused by the movement of the stiff deck during shaking.

Quantifying the responses of the investigated abutment-backfill configurations; the left abutment receives a maximum residual earth pressure of  $400.7 \pm 40.4$  kPa/m at a depth of 3.0 m from the ground surface, with 40.4 kPa/m being the standard deviation. A maximum residual earth pressure of  $370.3 \pm 68.6$  kPa/m is developed at the same depth on the second abutment, i.e. abutment 2. In case of

mechanically stabilized backfills, higher residual earth pressures are observed at the lower part of the abutments. However, the residual values are slightly lower compared to the conventional backfills, reaching a maximum of  $338.7 \pm 5.6$  kPa/m and  $296.2 \pm 55.1$  kPa/m, for abutments 1 and 2, respectively, at a depth of 3.5-4.0 m from ground surface. The isolated abutments experience the lowest values of post-shaking residual earth pressures, i.e.,  $162.5 \pm 21.9$  kPa/m and  $196 \pm 25.0$  kPa/m for isolated abutments 1 and 2, respectively. The latter maximum residual values are observed near the footings of the abutments. The reported locations of maximum residual earth pressures are in line with observations from previous studies (Mitoulis *et al.* 2016).

Similar observations are made by comparing the maximum envelope earth pressures developed on the abutments during cyclic thermal loading of the deck (Fig. 11(c)) and subsequent ground shaking (Fig. 11(d)). With reference to the earth pressures caused by the cyclic thermal loading of the deck (Fig. 11(c)); the abutments with conventional and mechanically stabilized backfills, receive a maximum envelope earth pressure of 1200 kPa/m, and 750 kPa/m, respectively, at a depth of 3.0-3.5 m from ground surface. Significantly lower maximum envelope earth pressures are predicted on the isolated abutments, reaching a maximum of 280 kPa/m, i.e., one-fifth of the maximum envelope earth pressures developed on abutments with conventional backfills.

Higher maximum envelope earth pressures are also computed on the abutments with the conventional backfills, when the ground seismic shaking is considered (Fig. 11(d)). In particular, abutments 1 and 2 receive a maximum envelope earth pressure of  $644.0 \pm 33.6$  kPa/m and  $620.0 \pm 13.0$  kPa/m, respectively, at a depth 2.0-2.5 m from ground surface. In case of mechanically stabilized backfills, the

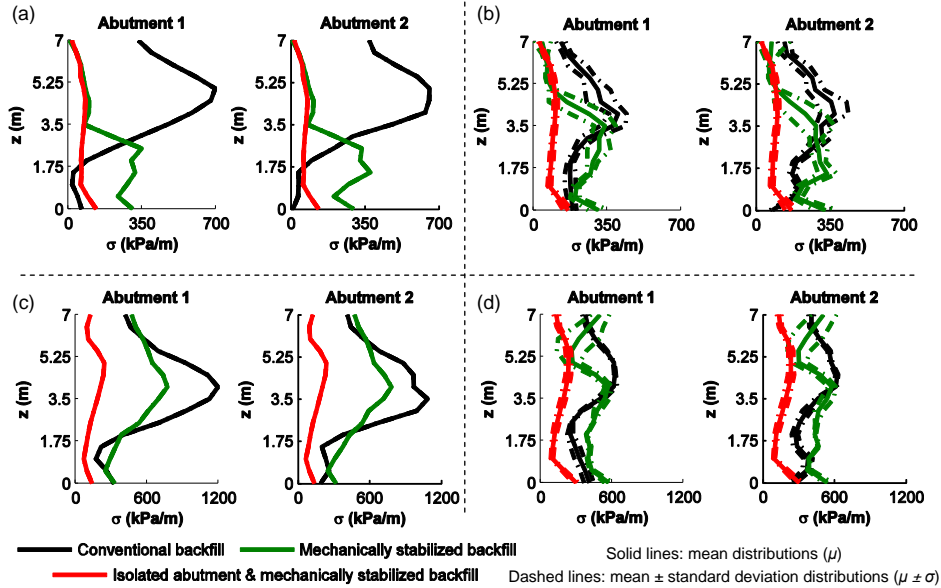


Fig. 11 Residual earth pressures distributions computed on the abutments at the completion of (a) cyclic thermal loading of deck and (b) ground seismic shaking. Maximum envelope distributions of earth pressures computed on the abutments during (c) cyclic thermal loading of the deck and (d) ground seismic shaking

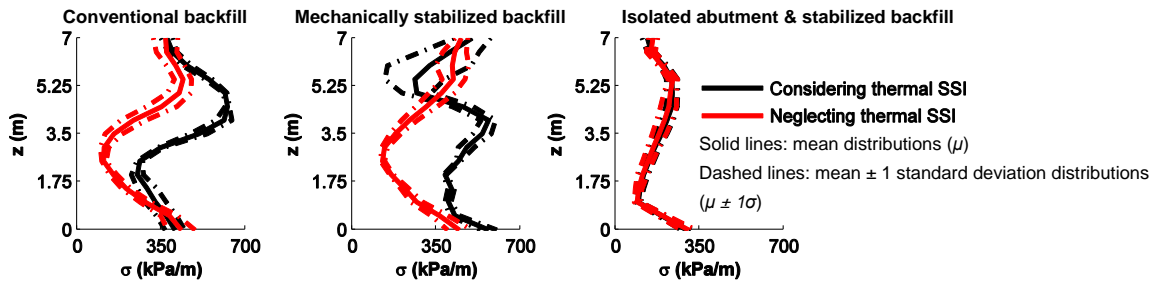


Fig. 12 Effect of pre-seismic thermal SSI on the maximum envelope distributions of earth pressures computed on the left-side abutments for the various backfill configurations investigated herein

envelope earth pressures reach a maximum of  $578.7 \pm 29.3$  kPa/m and  $567.2 \pm 30.9$  kPa/m on abutments 1 and 2, respectively, at a depth of 3.0 m from the ground surface. Isolated abutments 1 and 2 receive the lowest maximum envelope earth pressures, i.e.,  $270.0 \pm 30.2$  kPa/m and  $26.9$  kPa/m and  $294.0 \pm 22.2$  kPa/m, respectively, with these values being reported near the footings of the abutments.

Fig. 12 elaborates on the effect of pre-seismic thermal SSI on the maximum envelope earth pressures developed during ground seismic shaking on the left-side abutments for the various backfill configurations examined herein. Higher maximum envelopes of earth pressures are predicted on the abutments with conventional and mechanical stabilized backfills, when the pre-seismic thermal SSI is considered. On the contrary, the effect of pre-seismic thermal SSI is negligible in case of mechanically stabilized backfills supported by isolated abutments.

### 5.5 Bending moments on the IAB

Representative findings regarding the bending moments, developed on the structural components of the analyzed IAB, i.e., the deck, the piers and the abutments, during the cyclic thermal loading of the deck, as well as the ground

seismic shaking, are discussed in this section. The discussion focuses on the structural bending moments, since these actions are considered representative of the response and critical for the sizing and design of the structural elements. It is reminded that the stresses related to the prestressing of the deck were not considered in the analyses. Hence, the presented results account for the self-weight of the IAB, the additional permanent and variable traffic loads, the loading caused by the thermal loading of the deck and/or the loading due to the seismic action. The results presented hereafter refer to the unit width of the bridge, which was analyzed in this study.

Fig. 13(a) portrays time histories of the bending moments computed at the connection of left abutment with the deck during the cyclic thermal expansion and contraction of the deck. The bending moment, predicted in the case of the conventional backfill, reaches a maximum of 1890 kNm/m. A residual value of 1095 kNm/m is also identified at the completion of seasonal cyclic thermal expansion and contraction of the deck (i.e., 235 kNm/m higher than the bending moment due to dead and live loads). This residual response is associated to the yielding of the backfill soil during the thermal loading of the deck and the associated changes on the support that is offered by the

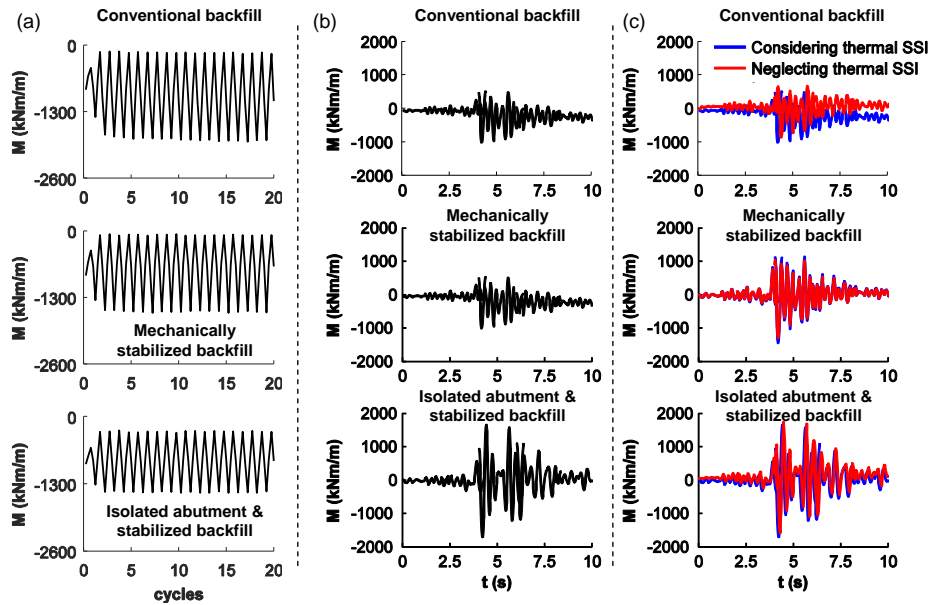


Fig. 13 Time histories of bending moments computed at the connection of the deck with the left abutment. (a) Bending moments due to cyclic thermal loading of the deck. (b) Seismic bending moments (dynamic part) computed for shaking with the Parnitha record, considering the pre-seismic thermal SSI effects. (c) Effect of pre-seismic thermal SSI on the seismic bending moments computed for shaking motion with the Parnitha record, scaled to 0.30 g

conventional backfill on the abutment. A similar response is reported in the case of the mechanically stabilized backfill, with the maximum and residual bending moments, however, being reduced to 1606 kNm/m and 750 kNm/m, respectively. The interjection of the compression inclusion between the abutment and the backfill results in a further reduction of maximum and residual bending moments, i.e., 1350 kNm/m and 650 kNm/m, respectively (null residual bending moment due to the thermal loading). It is worth noticing that the bending moments computed at the examined section of the IAB with the mechanically supported backfills under the permanent loads only were 5% lower than those predicted at the same section of the conventional IAB. The reduction reached 17% for the isolated IAB.

Fig. 13(b) depicts representative time histories of seismic bending moments computed at the connection of deck with left-side abutment during ground seismic shaking with the 1999 Parnitha earthquake record, scaled to  $PGA=0.30$  g. The results consider the pre-seismic thermal loading of the deck. Post-shaking residual values are identified on the predicted bending moments, for the cases of the conventional and the mechanically stabilized backfills. In particular, for the conventional backfill, the connection receives a maximum bending moment of 970 kNm/m, while a residual of 242 kNm/m is identified. Slightly lower maximum and residual bending moments are identified when the mechanically stabilized backfills are implemented (i.e., 960 kNm/m and 230 kNm/m, respectively). A higher dynamic bending moment is reported at the connection, in case of isolated abutments, reaching a maximum of 1770 kNm/m. This increase is due to the higher kinematic response that the isolated IAB exhibits compared to the conventional one, when subjected to the same shaking motion (see Table 2). On the contrary,

the residual bending moments in the case of isolated abutments are practically negligible.

Similarly to the earth pressures, the evolution of the dynamic bending moments is affected by the pre-seismic thermal SSI effects. Fig. 13(c) illustrates an example of this effect, by comparing the dynamic bending moments computed at the examined connection of the deck with the left abutment when the pre-seismic thermal SSI effects are considered or neglected. The differences on the predicted maximum and residual dynamic bending moments are generally higher in case of the abutment with the conventional backfill. On the contrary, the reported differences in case of the isolated abutment are negligible. The latter observation indicates again the decoupling of the seismic SSI effects from the thermal ones, when the abutment is isolated.

Fig. 14 compares the maximum and minimum envelope distributions of the total bending moments, computed on the deck, the piers and the abutments for all the analysed IAB-backfill systems, during the cyclic thermal loading of the deck. Generally, the response of the middle span of the deck and the piers under the cyclic thermal loading is not affected significantly by the design of the backfills. In line with the results presented above, the IAB with the conventional backfills experience the highest bending moments, while the isolated IAB receives the lowest bending moments. In particular, the maximum total bending moment induced on deck-abutments connections during thermal loading reach a maximum of 1904 kNm/m in case of the IAB with the conventional backfills. The bending moment predicted at the same location is reduced to 1704 kNm/m for the IAB with the mechanically stabilized backfills, i.e., a reduction of 12%. A further decrease of the maximum bending moment is observed in the case of the isolated IAB, with the maximum bending moment reaching

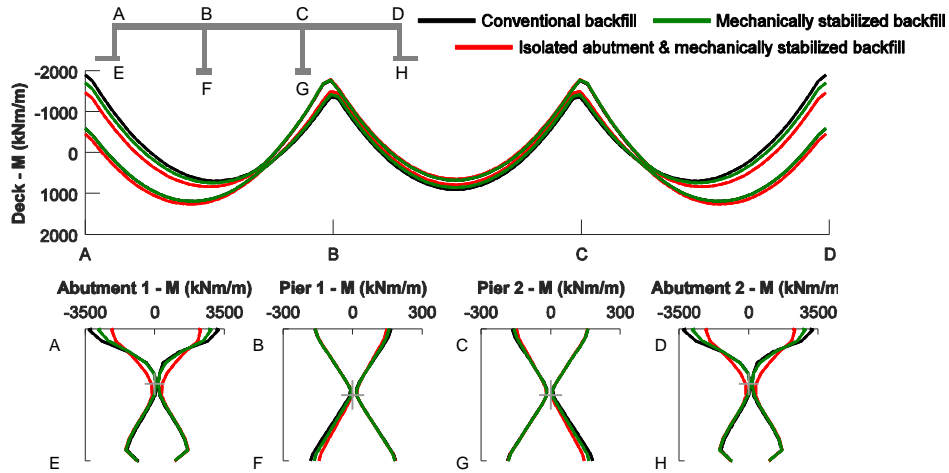


Fig. 14 Maximum and minimum envelope distributions of the total bending moments of the deck, the abutments and the piers of the IAB investigated herein, computed during the cyclic thermal loading of the deck

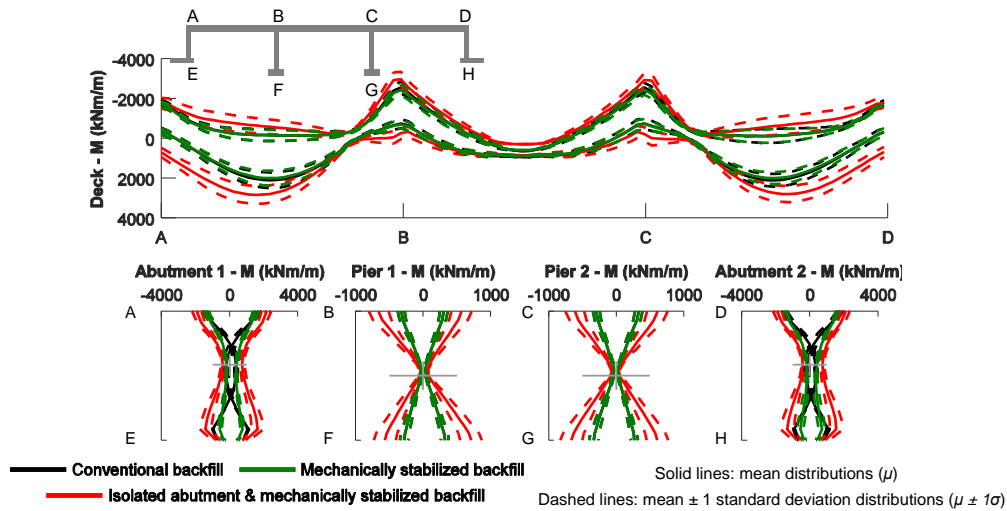


Fig. 15 Maximum and minimum envelope distributions of the total bending moments of the deck, the abutments and the piers of the IAB investigated herein, computed during the ground seismic shaking

1400 kNm/m, i.e., a decrease of 35% compared to conventional IAB. Similar observations are made by comparing the maximum bending moments computed on the abutments. The maximum bending moment on the abutments of the IAB with the conventional abutments reaches 3300 kNm/m, while for the IAB with mechanically stabilized backfills this maximum is 2810 kNm/m, i.e., a reduction of 28%. The maximum bending moment on the isolated abutments reaches a value of 2150 kNm/m, i.e., a reduction of 53% compared to the maximum bending moment of the conventional IAB.

Fig. 15 illustrates diagrams of the maximum and minimum envelope distributions of the total bending moments computed during ground seismic shaking along the deck, the abutments and the piers of the IAB for all the backfill configurations investigated herein. The solid lines refer to the mean distributions ( $\mu$ ) of the maximum or minimum envelope bending moments, while the dashed lines refer to the mean plus/minus one standard deviation ( $\mu \pm 1\sigma$ ) distributions, all computed by the corresponding envelope distributions that were estimated for the diverse

shaking motions. The effects of pre-seismic thermal SSI on the seismic performance of the IAB are considered in the presented results. A slight decrease (i.e., 5-10%) of the maximum and minimum envelopes of total bending moments of IAB with the mechanically stabilized backfills is observed compared to the ones of the IAB with the conventional backfills. On the contrary, higher envelope bending moments are reported on the elements of the isolated IAB compared to those predicted on the conventional IAB, due to the higher kinematic response of the former IAB during ground shaking (see Section 5.3). This increase is more evident for the deck-abutments connections and the piers and can be covered with proper designing and detailing of the sections. Quantifying the response in critical sections of the bridge; the maximum total bending moment that is induced on the deck-left abutment connection during ground seismic shaking reaches a maximum of  $-1796.7 \pm 149.2$  kNm/m in case of the IAB with the conventional backfills. The bending moment predicted at the same location is slightly reduced to  $-1706.0 \pm 111.2$  kNm/m for the IAB with the mechanically stabilized

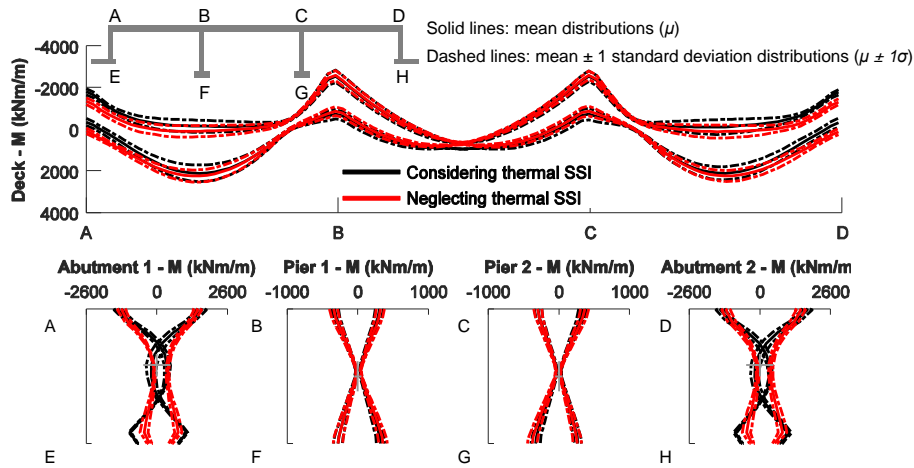


Fig. 16 Effect of pre-seismic thermal SSI on the maximum and minimum envelope distributions of bending moments computed on the IAB with conventional backfills

backfills, i.e., a reduction of 5.1%. An increase of the bending moment is observed in case of the isolated IAB with the maximum envelope bending moment reaching  $-1916.5 \pm 302.1$  kNm/m, i.e., 6.7% higher than the conventional IAB. Similar observations are made for the abutments. The left abutment receives a maximum envelope bending moment of  $-1568.8 \pm 145.7$  kNm/m in the case of IAB with the conventional backfills. This maximum increases by 22% (i.e.,  $-1909.2 \pm 276.3$  kNm/m) in the case of the isolated abutment. In the case of the midspans of the deck; the left-hand side midspan of the deck receives a maximum envelope bending moment of  $2102.8 \pm 393.9$  kNm/m in case of the IAB with the conventional backfills and  $3034.0 \pm 472.7$  kNm/m in the case of the IAB with the isolated abutments (i.e., an increase of 44%). It is worth noticing that the results presented in the Fig. 15 refer to envelope values, thus the comparisons should be considered as rather conservative. Moreover, the numerical predictions refer to a quite strong ground seismic shaking, with PGAs at the surface reaching 0.45 g to 0.65 g, depending on the amplification of the selected ground shaking motion.

Fig. 16 highlights the effect of pre-seismic thermal SSI on the maximum and minimum envelopes of total bending moments computed during ground seismic shaking on the structural elements of the IAB with the conventional abutments. Higher envelopes of total bending moments are predicted on the abutments, as well as on the deck near the connections with the abutments, when the pre-seismic thermal SSI effects are considered. The differences can be as high as 20%. Contrary to the conventional abutment-backfill configurations, the pre-seismic thermal SSI effects had a negligible effect on the envelopes of bending moments reported during ground seismic shaking, in the case of the IAB with the isolated abutments.

Summarizing, the isolated IAB is expected to experience lower bending moments during cyclic thermal loading of the deck, compared to the IAB with conventional backfills. The reduction of the bending moment on the structural elements of the isolated IAB is a quite favourable effect of the decoupling of the abutments from the backfills and concerns all bridges, especially these with long spans.

With reference to the IAB in seismic prone areas; during severe ground seismic shaking, isolated IAB are expected to deform more freely, thus experiencing higher seismic actions, compared to the conventional IAB. The increased seismic bending moments of the isolated IAB are counterbalanced by other benefits of the isolation, i.e., lower bending moments for the structural elements during thermal loading, lower post-shaking residual bending moments on the structural elements, smaller earth pressures on the abutments and reduced permanent deflections of the backfill. Additionally, the seismic response of conventional backfills and the IAB are difficult to be predicted accurately, especially in cases where significant thermal SSI effects have been preceded. On the contrary, the seismic response of an isolated IAB is much more predictable, since the uncertainty related to the non-linear response of the backfills is significantly mitigated in this case, due to the decoupling of the seismic SSI effects from the pre-seismic thermal ones. This may allow for a proper evaluation of the seismic response of the IAB and therefore an adequate seismic design of the structural elements (e.g., by providing sufficient ductility on of the piers and the abutments of the bridge).

## 6 Conclusions

The response of IAB under thermal loading of the deck and subsequent ground seismic shaking in the longitudinal direction was investigated in this paper by means of numerical analyses of a representative backfill-integral bridge-foundation-soil system. Particular emphasis was placed on the effect of pre-seismic thermal SSI on the seismic performance of the IAB, as well as on the ability of various abutment backfill designs, to minimize the dependence of seismic SSI effects from the thermal ones. The key findings of this study are summarized in the following:

- The cyclic thermal loading of the deck led to significant soil yielding at the top of the conventional backfills, which in turn resulted in high residual

swelling and settlement vertical deflections of the backfills surfaces. These phenomena were less pronounced for the mechanically stabilized backfills, while the backfills that were supported by the isolated abutments responded almost elastically. Additionally, the pre-seismic thermal SSI effects dominated the post-seismic residual distortions of the conventional backfills, while the effect of pre-seismic thermal SSI on the post-seismic distortions of the backfills, supported by the isolated abutments, was almost negligible.

- The cyclic thermal loading of the deck, induced significant deformations on the integral abutments. Similarly, the ground seismic shaking resulted in significant deformations of the integral abutments. The consideration of different backfill systems affected the seismic drifts of the walls of the abutments, with higher values being reported for the isolated abutments. Additionally, the pre-seismic thermal SSI effects resulted in a decrease of the maximum seismic drifts of the walls of the abutments with conventional backfills, compared to the cases where these effects were neglected. On the contrary, the effect of pre-seismic thermal SSI on the seismic drifts of isolated abutments was negligible.

- High earth pressures were reported on the walls of the abutments with conventional backfills during the thermal loading of the deck. On the contrary, the isolated abutments received considerably lower earth pressures during this loading condition. Similar observations were made for the ground seismic shaking, with the earth pressures magnitudes being generally lower compared to those reported during the thermal loading. Furthermore, higher earth pressures were developed on the abutments with conventional backfills during ground shaking, when the pre-seismic thermal SSI effects were considered. The decoupling of the backfills from the isolated abutments led to a negligible effect of thermal SSI on the seismic earth pressures. The above trends should be partly attributed to the development of residual earth pressures on the walls of the abutments during both loading conditions. Indeed, significant residual earth pressures were developed on the abutments with the conventional backfills, as a result of their high yielding response reported during both loading conditions. These residual earth pressures were reduced for the mechanically stabilized backfills, while they were negligible for the isolated backfills.

- The bending moments computed on the structural elements of the IAB with mechanically stabilized backfills during the cyclic thermal loading of the deck were reduced compared to the conventional IAB, while the isolated IAB experienced the lowest bending moments. With reference to the seismic response; a slight decrease was observed on the bending moments of IAB with the mechanically stabilized backfills compared to the ones predicted for the case of the conventional IAB. Additionally, higher envelope bending moments were reported on the elements of the isolated IAB (particularly on the deck-abutments connections and the piers) compared to those predicted on the conventional IAB, due to the higher kinematic

response of the former IAB during ground shaking. On the other hand, the residual bending moments added by ground seismic shaking on the structural elements of the isolated IAB were practically negligible, compared to the conventional IAB, where significant post-shaking residual bending moments were reported. Finally, the pre-seismic thermal SSI led to higher bending moments on the structural elements of the conventional IAB during the subsequent ground seismic shaking (i.e., on the abutments and near the connections of the abutments with the deck), compared to the cases where the thermal SSI effects were neglected. This latter effect was negligible in case of the isolated abutments.

The general conclusion is that significant SSI effects may be mobilized between the IAB and the backfills during the cyclic thermal loading of the deck and the subsequent ground seismic shaking, which may be interrelated in some cases. The quantification of these effects is only possible on a case to case basis, as the above phenomena are dependent to a greater or lower extent by a number of parameters, e.g. length of the bridge, type, height and foundation of the integral abutment, soil type of the backfills and the foundation soil, existence of secondary structural elements (e.g., wing walls or approach slab). However, the main observations and insights provided herein may be considered valid for this type of bridges, at least on a quantitative basis. Along these lines, the pre-seismic thermal SSI effects should be accounted for in the seismic analysis of IAB with conventional cohesionless backfills. Further investigation is needed to propose simplified, yet adequate, models towards this direction. On the contrary, the analysis of the SSI effects, caused by thermal and seismic loadings, can be decoupled in cases of IAB with isolated backfills.

## References

- ABAQUS (2012), Theory and Analysis User's Manual, Version 6.12, Dassault Systèmes SIMULIA, Providence, USA.
- Agalianos, A., Sakellariadis, L. and Anastasopoulos, I. (2017), "Simplified method for the assessment of the seismic response of motorway bridges: longitudinal direction-accounting for abutment stoppers", *Bull. Earthq. Eng.*, **15**(10), 4133-4162.
- Argyroudis, S., Kaynia, A.M. and Pitilakis, K. (2013), "Development of fragility functions for geotechnical constructions: application to cantilever retaining walls", *Soil. Dyn. Earthq. Eng.*, **50**, 106-116.
- Argyroudis, S., Palaiochorinou, A., Mitoulis, S.A. and Pitilakis, D. (2016), "Use of rubberised backfills for improving the seismic response of integral abutment bridges", *Bull. Earthq. Eng.*, **14**(12), 3573-3590.
- Athanasopoulos-Zekkos, A., Lamote, K. and Athanasopoulos, G.A. (2012), "Use of EPS geofoam compressible inclusions for reducing the earthquake effects on yielding earth retaining structures", *Soil. Dyn. Earthq. Eng.*, **41**, 59-71.
- Aviram, A., Mackie, K.R. and Stojadinovic, B. (2008), "Effect of abutment modelling on the seismic response of bridge structures", *Earthq. Eng. Eng. Vib.*, **7**(4), 395-402.
- Baptiste, K.T., Kim, W. and Laman, J.A. (2011), "Parametric study and length limitations for prestressed concrete girder integral abutment bridges", *Struct. Eng. Int.*, **21**(2), 151-156.
- Bardet, J.B., Ichii, K. and Lin, C.H. (2000), "EERA: a computer

- program for equivalent-linear earthquake site response analyses of layered soil deposits”, Report, Department of Civil Engineering Department of Civil Engineering, University of Southern California, Los Angeles, USA.
- Bloodworth, A., Xu, M., Banks, J. and Clayton, C. (2012), “Predicting the earth pressure on integral bridge abutments”, *J. Bridge Eng.*, **17**(2), 371-381.
- Callisto, L. and Soccodato, F.M. (2010), “Seismic design of flexible cantilevered retaining walls”, *J. Geotech. Geoenviron. Eng.*, **136**(2), 344-354.
- Darendeli, M. (2001), “Development of a new family of normalized modulus reduction and material damping curves”, Ph.D. Dissertation, University of Texas, Austin.
- EN 1991-2 (2003), Eurocode 1: Actions on Structures. Part 2: Traffic loads on bridges, European Committee for Standardization, Brussels, Belgium.
- EN 1991-5 (2003), Eurocode 1: Actions on Structures. Part 1.5: General Actions-Thermal Actions, European Committee for Standardization, Brussels, Belgium.
- EN 1997-1 (2004), Eurocode 7: Geotechnical Design. Part 1: General Rules, European Committee for Standardization, Brussels, Belgium.
- EN 1998-1 (2004), Eurocode 8: Design of structures for earthquake resistance. Part 1: General Rules, Seismic Actions and Rules for Buildings, European Committee for Standardization, Brussels, Belgium.
- EN 1998-2 (2005), Eurocode 8: Design of Structures for Earthquake Resistance. Part 2: Bridges, European Committee for Standardization; Brussels, Belgium.
- EN 1998-5 (2005), Eurocode 8: Design of Structures for Earthquake Resistance. Part 5: Foundations, Retaining Structures and Geotechnical Aspects, European Committee for Standardization, Brussels, Belgium.
- England, G.L. (2005), “A thermal displacement compensation unit for integral bridges”, Patents, Bridge Structures, P.N., CA 2605437 A1.
- England, G.L. and Tsang, N. (2001), “Towards the design of soil loading for integral bridges-experimental evaluation”, Department of Civil and Environmental Engineering, Imperial College, London, UK.
- England, G.L., Tsang, N. and Bush, D. (2000) *Integral Bridge: A Fundamental Approach to the Time-temperature Loading Problem*, Thomas Telford, London, UK.
- England, G.L., Tsang, N., Ferreira, P.M.V. and Teixeira, B. (2007), “Some design improvements for integral bridges”, *Proceedings of the 5th International Conference on Current and Future Trends in Bridge Design, Construction and Maintenance*, Beijing, China.
- Erhan, S. and Dicleli, M. (2015), “Comparative assessment of the seismic performance of integral and conventional bridges with respect to the differences at the abutments”, *Bull. Earthq. Eng.*, **13**(2), 653-677.
- Evangelista, A., di Santolo, A.S. and Simonelli, A.L. (2010), “Evaluation of pseudostatic active earth pressure coefficient of cantilever retaining walls”, *Soil Dyn. Earthq. Eng.*, **30**(11), 1119-1128.
- Hashash, Y.M.A. and Park, D. (2002), “Viscous damping formulation and high frequency motion propagation in non-linear site response analysis”, *Soil Dyn. Earthq. Eng.*, **22**(7), 611-624.
- Helwany, S. (2007), “Evaluation of bridge approach settlement mitigation methods”, Report 07-14, Wisconsin Highway Research Program, University of Wisconsin-Milwaukee, USA.
- Highways Agency (1995), BD 57: Design for Durability, HMSO, London, UK.
- Highways Agency (2000), BA 42: The Design of Integral Bridges, HMSO, London, UK.
- Highways Agency (2001), DB 37: Loads for Highway Bridges, DMRB 1.3.14, HMSO, London, UK.
- Horvath, J. (2010), “Lateral pressure reduction on earth-retaining structures using geofoams: Correcting some misunderstandings”, *Proceedings of ASCE Earth Retention Conference 3*, Bellevue, Washington, August.
- Humphrey, D. (2010), “Civil engineering applications using tire derived aggregate (TDA)”, Research Report No. DRRR-2011-038, California Waste Management Board, California, USA.
- Humphrey, D. and Blumenthal, M. (2011), “The use of tire-derived aggregate in road construction applications”, *Proceedings of Green Streets & Highways Conference ASCE*, Denver, Colorado, November.
- IABSE (2011), “Special issue on integral bridges”, *Struct. Eng. Int.*, **2**.
- INTAB (2010), “Economic and durable design of composite bridges with integral abutments”, Research Report No. RFSP2-08065, European Commission, Brussels.
- Kappos, A.J. and Sextos, A.G., (2009), “Seismic assessment of bridges accounting for nonlinear material and soil response and varying boundary conditions”, *NATO Science for Peace and Security Series C: Environmental Security*, **3**, 195-208.
- Kotsoglou, A. and Pantazopoulou, S., (2007), “Bridge-embankment interaction under transverse ground excitation”, *Earthq. Eng. Struct. Dyn.*, **36**(12), 1719-1740.
- Kotsoglou, A. and Pantazopoulou, S., (2009), “Assessment and modelling of embankment participation in the seismic response of integral abutment bridges”, *Bull. Earthq. Eng.*, **7**, 343-361.
- LaFave, J., Riddle, J., Jarrett, M., Wright, B., Svatora, J., An, H. and Fahnestock, L., (2016), “Numerical simulations of steel integral abutment bridges under thermal loading”, *J. Bridge Eng.*, doi: 10.1061/(ASCE)BE.1943-5592.0000919.
- Lemnitzer, A., Ahlberg, E., Nigbor, R., Shamsabadi, A., Wallace, J. and Stewart, J. (2009), “Lateral performance of full-scale bridge abutment wall with granular backfill”, *J. Geotech. Geoenvironm. Eng.*, **135**(4), 506-514.
- Lysmer, J. and Kuhlemeyer, R.L. (1969), “Finite dynamic model for infinite media”, *J. Eng. Mech. Div.*, **95**(4), 859-878.
- Mistry, V.C. and Mangus, A. (2006), “Get in, stay in, get out, stay out”, Research Report No. FHWA-HRT-2006-001, **70**(3), Federal Highway Administration, Department of Transportation, Washington, USA.
- Mitoulis, S.A. (2012), “Seismic design of bridges with the participation of seat-type abutments”, *Eng. Struct.*, **44**, 222-233.
- Mitoulis, S.A. and Tegos, I.A., (2011), “Two new earthquake resistant integral abutments for medium to long-span bridges”, *Struct. Eng. Int.*, **21**(2), 157-161.
- Mitoulis, S.A., Palaiochorinou, A., Georgiadis, I. and Argyroudis, S., (2016), “Extending the application of integral frame abutment bridges in earthquake-prone areas by using novel isolators of recycled materials”, *Earthq. Eng. Struct. Dyn.*, **45**(14), 2283-2301.
- Mitoulis, S.A., Tegos, I.A. and Stylianidis, K.C., (2010), “Cost-effectiveness related to the earthquake resisting system of multi-span bridges”, *Eng. Struct.*, **32**(9), 2658-2671.
- Pistolas, G.A., Tsinaris, A., Anastasiadis, A. and Ptilakis, K. (2014), “Undrained dynamic properties of Hostun sand”, *Proceedings of 7<sup>th</sup> Greek Geotechnics Conference*, Greece Hellenic Society of Soil Mechanics and Geotechnical Engineering, Athens, November. (in Greek)
- Potyondy, J.G. (1961), “Skin friction between various soils and construction materials”, *Géotechnique*, **11**(1), 339-353.
- Quinn, B.H. and Civjan, S.A. (2016), “Parametric study on effects of pile orientation in integral abutment bridges”, *J. Bridge Eng.*, doi: 10.1061/(ASCE)BE.1943-5592.0000952.
- Schanz, T. and Vermeer, P.A. (1996), “Angles of friction and dilatancy of sand”, *Géotechnique*, **46**(1), 145-151.

- Shamsabadi, A., Rollins, K.M. and Kapuskar, M. (2007), "Nonlinear soil-abutment-bridge structure interaction for seismic performance-based design", *J. Geotech. Geoenviron. Eng.*, **133**(6), 707-720.
- Shamsabadi, A., Xu, S.Y. and Taciroglu, E. (2013), "A generalized log-spiral-Rankine limit equilibrium model for seismic earth pressure analysis", *Soil Dyn. Earthq. Eng.*, **49**, 197-209.
- Springman, S.M., Norrish, A. and Ng, C.W.W. (1996), "Cyclic loading of sand behind integral bridge abutments", Research Report No. 146, Transport Research Laboratory, Berkshire, UK.
- Tsinidis, G., Ptilakis, K. and Madabhushi, G. (2016b) "On the dynamic response of square tunnels in sand", *Eng. Struct.*, **125**, 419-437.
- Tsinidis, G., Ptilakis, K., Madabhushi, G. and Heron, C. (2015) "Dynamic response of flexible square tunnels: Centrifuge testing and validation of existing design methodologies", *Géotechnique*, **65**(5), 401-417.
- Tsinidis, G., Rovithis, E., Ptilakis, K. and Chazelas, J.L. (2016a), "Seismic response of box-type tunnels in soft soil: Experimental and numerical investigation", *Tunn. Undergr. Space Tech.*, **59**, 199-214.
- Tubaldi, E., Barbato, M. and DallAsta, A. (2010), "Transverse seismic response of continuous steel-concrete composite bridges exhibiting dual load path", *Earthq. Struct.*, **1**(1), 21-41.
- Zanini, M.A., Pellegrino, C., Morbin, R. and Modena, C. (2013), "Seismic vulnerability of bridges in transport networks subjected to environmental deterioration", *Bull. Earthq. Eng.*, **11**(2), 561-579.
- Zhang, J. and Makris, N. (2002), "Seismic response analysis of highway overcrossings including soil-structure interaction", *Earthq. Eng. Struct. Dyn.*, **31**(11), 1967-1991.

AT